Journal of Petroleum Science and Engineering 133 (2015) 695–704

Contents lists available at ScienceDirect

Journal of Petroleum Science and Engineering

journal homepage: www.elsevier.com/locate/petrol

Permeability evolution of propped artificial fractures in coal on injection of CO_2

Hemant Kumar [a,*], Derek Elsworth [a], Jishan Liu [b], Denis Pone [c], Jonathan P. Mathews [a]

[a] John and Willie Leone Department of Energy and Mineral Engineering, EMS Energy Institute, and G3 Center, Pennsylvania State University, University Park, PA 16802, USA
[b] School of Mechanical Engineering, University of Western Australia, WA 6009, Australia
[c] ConocoPhillips, Bartlesville, OK, USA

ARTICLE INFO

Article history:
Received 9 September 2014
Received in revised form
21 April 2015
Accepted 8 July 2015
Available online 9 July 2015

Keywords:
Permeability
Coal
Proppant
Enhanced coalbed methane
Modeling

ABSTRACT

Proppants are often utilized during hydraulic fracturing to aid the retention of the fracture aperture. However, for coal the permeability enhancement may be mitigated due to proppant embedment within the natural/artificial fractures of coalbed methane reservoirs. This process may become increasingly complex if CO_2 is injected in the reservoir for enhanced recovery. The reduction in effective fracture aperture occurs under the influence of overburden stress either when CO_2-induced coal softening causes proppant penetration into the coal fracture surface or coal swelling encroaches into the propped facture. Here permeability transformations at simulated in situ conditions were evaluated through a suite of laboratory experiments conducted on split-cores of high-rank coals. A single smooth-surface saw-cut fracture was created and the permeability evolution measured for both non-sorbing (He) and sorbing (CO_2) gases at constant applied confining stress of 10 MPa. Permeability was also measured for the idealized case of a uniform monolayer of #70–140 mesh quartz sand proppant sand introduced within the saw-cut fracture for coal. The increase in He permeability was as high as ~10 fold over the unpropped fracture for a monolayer of proppant sandwiched within the coal. A similar increase in permeability with the addition of proppant was observed in the case of sorptive gas (CO_2) for coal. For He there was an exponential increase in permeability with increasing gas pressure (p=1–6 MPa) for coal without proppant, as expected, as the effective stress on the core was reduced. However, with CO_2 the permeability decreased in the 1–4 MPa pressure range due to either coal swelling or softening or their combination but increased above 4 MPa due to reduced effective stress.

Optical profilometry pre- and post-exposure was used to quantify any surface deformation due to proppant embedment. Comparison of the fracture surface before and after showed only infrequent new isolated pits, similar to the size of the proppant grains. The slight increase in surface roughness following exposure to CO_2 was presumed due to irreversible rearrangement of the coal structure due to CO_2 uptake then loss. A mechanistic model explains the evolution of permeability in a propped artificial fracture due to interaction with a sorbing gas (CO_2). Permeability evolves with a characteristic "U-shaped" trend with increasing gas pressure at constant confining stress – permeability reduces to a minimum at approximately double the Langmuir pressure flanked by elevated permeabilities at either low sorptive states (low p) or at low effective stress (high p). An excellent fit is recovered between model and experimental observations.

1. Introduction

Hydraulic fracturing is extensively used for tight shale and sand reservoirs to enhance the permeability. Also, low permeability coalbed reservoirs are often considered good candidates for hydraulic fracturing for economical production of coalbed methane (Davidson et al., 1995; Holditch et al., 1988). There are many studies which have explored various processes e.g. permeability evolution, proppant crushing, proppant embedment, proppant digenesis, movement of fines in fractures in the context of hard rocks. Prior experimental (Piggott and Elsworth, 1993; Walsh, 1981) and analytical evaluations (Bai and Elsworth, 1994; Elsworth and Yasuhara, 2010; Yasuhara and Elsworth, 2008; Yasuhara et al., 2006) of fractured rocks indicate that permeability is strongly influenced by the variation in mechanical, chemical, thermal, and hydraulic processes.

* Corresponding author. Current address: Chevron-ETC, Houston, Texas-77002, USA.

http://dx.doi.org/10.1016/j.petrol.2015.07.008
0920-4105/

Proppant embedment and fracture closure have received additional attention for hard rock as optimization of proppant effectiveness is necessary to prevent fracture closure. Mechanisms of fracture conductivity impairment have been explored including the roles of fines migration (Pope et al., 2009), proppant diagenesis (LaFollette and Carman, 2010; Lee et al., 2010), proppant crushing (Terracina et al., 2010), and reduction in fracture aperture due to the embedment of proppant grains into the surface of the hydraulic fracture (Freeman et al., 2009; Lacy et al., 1997). Proppant embedment studies on 20/40 and 40/60 mesh Ottawa sand and sintered bauxite indicate that the embedment is primarily modulated by closure stress, proppant size and fluid viscosity (Lacy et al., 1997). The reduction in fracture conductivity at higher effective stresses occurs due to generation of proppant-fines in hard rocks (such as granite). The reduction in conductivity may be up to 60% in rock (Lacy et al., 1997) and perhaps higher for coal. With higher temperatures, extended duration of stress loading, and pressurized fluid saturation levels may accelerate the fines generation or proppant embedment (Freeman et al., 2009). An increase in temperature decreases the fracture conductivity due to the thermal expansion of asperities under mechanical constraints (Stoddard et al., 2011). The time dependent tensile strength, proppant hardness, and fatigue failure of proppant under reservoir conditions are known to affect proppant efficacy (LaFollette and Carman, 2010; Freeman et al., 2009). The fracture treatment may also be impacted by proppant-diagenesis, which evolves as a result of mineral dissolution, transport and re-precipitation in the particle interstices. Thus various mechanisms may be responsible for porosity and permeability loss in proppant packs within hard rocks (Lee et al., 2010) if the proppant layer is sufficiently thick so that the surface asperities do not play a significant role (Stoddard et al., 2011).

Although the behavior of propped artificial fractures in hard rocks has been well explored, the response of proppant packs in soft sorbing media (coal) is poorly understood due to the complex range of behaviors. Coal matrix swells and develops strains on exposure to CO_2 which may result in reduction of fracture-apertures therefore lowering the permeability (Karacan, 2003, 2007; Kumar et al., 2014). Also, it is known that coal can soften upon exposure to "good" solvents becoming ductile or plastic and easily deformable (Brenner, 1984, 1985). Presumably, both coal-CO_2 *swelling* and coal *softening* may result in effective aperture reduction either due to coal encroaching in the proppant void spaces (via coal swelling), or due to the proppant penetrating the coal (via coal softening). The response of coals is more complex as they are typically: (1) softer than the proppant grain, (2) exhibit swelling on exposure to CO_2, (3) weaken upon interaction with CO_2 developing dynamic strains (Perera and Ranjith, 2012; Viete and Ranjith, 2006), and (4) perhaps soften. These processes are expected to result in permeability transformations.

Here the permeability evolution of an artificial saw-cut "fracture" in bituminous and anthracite cores both with and without proppant was explored for both inert helium (He) and sorbing carbon dioxide (CO_2) as permeating gases. Permeability evolution was determined using the pulse-transient technique at constant applied confining stress (10 MPa) for non-propped and propped fractures at different (saturated) gas pressures. The evolution of surface morphology was evaluated using optical profilometry to aid in establishing the role, if any, of coal softening on permeability evolution. We also used these observations to constrain mechanistic models of permeability evolution of propped fractures in sorbing media.

2. Experimental methods

Cylindrical cores of bituminous and anthracite rank coals were longitudinally-split to produce a single diametral artificial fracture. Fluid (gas) injection experiments were performed on the fracture in these cores in both non-propped and propped mode with samples stressed to in situ conditions but under ambient laboratory temperature (20 °C). The gases He and CO_2 were used as permeants to investigate the role of swelling/softening and effective stress on the dynamic evolution of permeability.

2.1. Samples

Two coals were used in the experiments: bituminous coal from the Uinta Basin, Colorado and anthracite from Pennsylvania. The coal block samples were cored horizontally (parallel to bedding) to produce the core plugs. The calorific value of sampled bituminous and anthracite coals were 12,000 and 14,286 BTU/lb (ASTM International D388, 2005) on a dry basis, respectively. The fixed carbon, volatile material and ash yield on a dry basis are 57%, 38%, 5% for bituminous and 86%, 7%, 4% for anthracite coals (ASTM International D7582, 2010). The moisture content of the coals are 5% and 2% respectively (ASTM International D3302/D3302M-10, 2010).

Six cylindrical cores of 2.5 cm diameter and 5 cm length were obtained and their ends cut to obtain flat surfaces (Fig. 1). Cores were cut in to two halves (horizontally lengthwise) using a thin diamond coated blade to produce smooth opposing surfaces forming an idealized fracture. The cut-surfaces of the coal were polished to remove the minor saw indents. Fine sand paper (#400) to very fine cotton cloth with alumina powders from 0.3 μm to 0.05 μm were used to polish the coal surface (ASTM International D5671, 2011). Surface roughness was quantified by optical profilometry (Kumar et al., 2009; Rousseau et al., 2010). The split-cores were re-mated either without or with a uniform monolayer of 70–140 mesh proppant sand. The cores were then wrapped in aluminum foil (to prevent diffusive loss of CO_2) (Kumar et al., 2011) and sheathed in a latex jacket before being enclosed in a pressurized core holder for the permeability experiments.

2.2. Apparatus

An apparatus in simple tri-axial configuration was used for the injection of gases under predefined effective stress paths and capable of concurrent measurement of permeability (Fig. 2). All experiments were completed under a constant applied total stress with same axial and confining stresses. The apparatus comprised a tri-axial cell to confine the sample at prescribed stresses, an axial strain gauge to monitor the shrinkage or swelling in the axial direction, ISCO syringe pumps to apply stresses and to measure volume strains (axial and confining), pressure transducers to monitor the upstream and downstream reservoir pressures and a data acquisition system. Additional details of the equipment are described elsewhere (Kumar et al., 2012). A transient pulse test method (described in Section 2.4) was used to determine the saturated sample permeability. Permeability was evaluated from the rate of pressure decay/gain in the upstream/downstream reservoirs (Brace et al., 1968) assuming no additional sorption occurs in the saturated sample by insignificantly small pressure pulse during the experiments.

Both pre- and post-experiment an optical profilometer (Zygo NewView™ 7300) was used to quantify the surface indentation caused by stressing of the sample and the presence of sorptive gas pressure. In the interferometer a light beam is split into two paths. One path of light impinges on the specimen surface and is reflected. The other is reflected from a reference mirror. Reflections from these surfaces are recombined and projected onto an array detector to determine path differences by interference. This enables surface topography to be resolved to fractions of the

Fig. 1. A typical cylindrical sample's polished fracture surface.

wavelength of light. Resolution in the plane and vertical to the plane is 2 μm and 0.1 μm respectively. A 10× objective was used with 0.5× zoom length. The surface topology of a region 7 mm × 8 mm was obtained by stitching-together ~30 micrographs at high resolution with the field of view overlapping by ~20%.

Table 1
Suite of variables and prescribed ranges utilized in the experiments, for gas pressure P_p, permeability k, axial stress σ_1, confining stress σ_3, and axial strain ε_a.

Experimental variables	Experimental range
Temperature (T)	Constant
Gas pressure (*Pp*, MPa)	1–6
Axial stress (σ_1, MPa)	10
Confining stress (σ_3, MPa)	10
Gas type	He, CO_2

2.3. Procedures

The coal cores were held within the tri-axial core holder and stresses were applied. The experiments were conducted at constant confining stress of 10 MPa (equivalent to an effective stress at ~1000 m or ~3300 feet depth). The permeability experiments included injection of He and CO_2 in both non-propped and propped coal fractures. The suite of experiments were conducted on bituminous and anthracite coal cores to explore the evolution permeability of an artificial fracture as a result of injection of either inert (He) or sorbing (CO_2) gas. Table 1 provides the ranges of experimental variables.

The experimental protocol sequence was performed under constant isotropic stress with incremental gas pressures. The suite of experiments included:

1. *Non-propped fracture – He permeability*: Helium (considered to be a non-adsorbing fluid) was circulated in the non-propped coal sample.
2. *Non-propped fracture – CO_2 permeability*: The sample is at equilibrium with CO_2 and permeability measured by transient pulse test at different saturated conditions (gas pressures 1–6 MPa).
3. *Propped fracture – He permeability*: The artificial fracture in the sample was propped open with a monolayer of proppant. Helium was injected in the sample at different gas pressures and the permeability determined.
4. *Propped fracture – CO_2 permeability*: The sample was vented

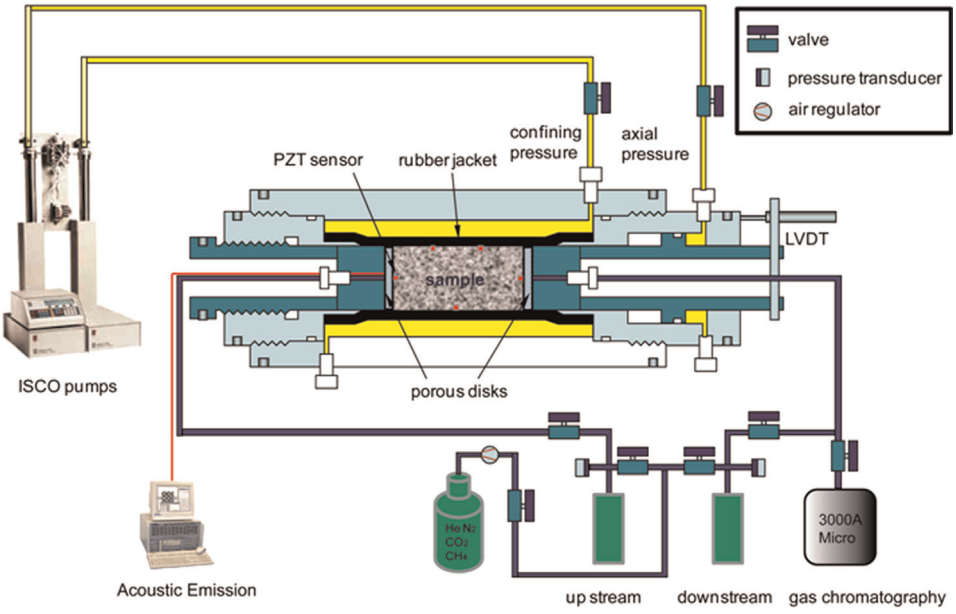

Fig. 2. Schematic of transient pulse test permeability apparatus.

overnight to the atmosphere and permeated using CO_2. The permeability was measured on the saturated sample.

Surface micrographs were captured using optical interferometry and contain information on the surface roughness including the height/depth of the surface features. The surface micrographs were obtained for the surface both before and after (<30 min) the experimental suite for a single sample. To allow comparison, same sample is used for the entire experimental suite for a given coal. The samples were taken out of the tri-axial cell after measuring the He and CO_2 permeability under non-propped condition. Then, a single layer of proppant was sandwiched in the fracture and the sample was set in the tri-axial cell again for completing the permeability tests (He and CO_2) under propped condition.

2.4. Data processing

The transient pulse test method was utilized to evaluate permeability (Brace et al., 1968). In a typical run, a coal core was packed and placed under axial and radial stress applied as shown in Fig. 2. A mild vacuum ($\sim$25 mm Hg) was applied to evacuate the air from the sample reservoir system. The core including both upstream and downstream reservoirs were gas saturated (He or CO_2) to an arbitrary chosen saturation pressure before applying the pressure pulse to the upstream side. The pulse was allowed to flow from upstream side to downstream side through the core until upstream and downstream pressures were approximately equal. This state is defined as the equilibrium gas pressure. The equilibrium pressure for the system is equal to p_{down^0} before applying pressure pulse to upstream. The pressure pulse is significantly smaller ($<10\%$) than the initial gas pressure in the system to limit the excursion of the effective stress. As the Langmuir pressures for the coals are in the Mega-Pascal range (0–3 MPa) (Kumar et al., 2012) we assume that there is insignificant additional adsorption for an increment in gas pressure that is less than 10% of the equilibrium pressure. Also, the small pressure pulse allows avoiding inertial effects. The progress of pressure loss in the upstream reservoir and pressure gain in the downstream reservoir were recorded to enable permeability to be determined. This process was repeated until the predetermined value of gas pressure was achieved. The pressure–time profile from the experiment was used to obtain permeability, k (Brace et al., 1968), as

$$k = \frac{\gamma.\,\mu.\,L.\,V_{up}V_{down}}{P_{eq}.\,A.\,\left(V_{up}+V_{down}\right)} \tag{1}$$

where permeability k (m^2) is calculated from the decay parameter γ (s^{-1}) for a known gas viscosity μ (Pa s), sample length L (m), equilibrium pressure at the end of the experiment P_{eq} (N/m^2) and cross sectional area of the specimen A (m^2). This is relative to upstream/downstream reservoir volumes $V_{up/down}$ (m^3), measured initial pressure $p_{up/down^0}$ (N/m^2) and transient upstream/downstream reservoir pressures $p_{up/down}$ (N/m^2) and modulated by the slope of the pressure change curve with time as

$$\gamma = \frac{\log\left(\frac{d\left(p_{up}-p_{down}\right)}{\left(p_{up^0}-p_{down^0}\right)}\right)_t}{dt} \tag{2}$$

where γ is the slope of pressure change $log\left(\frac{d\left(p_{up}-p_{down}\right)}{\left(p_{up^0}-p_{down^0}\right)}\right)$ versus time, usually represented as a semi-log plot. This method yields a single value of permeability for a single pulse.

Pressure-decay in the upstream reservoir and complementary pressure-gain in the downstream reservoir for a typical pulse test in moist coal with non-adsorbing (He) gas is shown in Fig. 3. Pulse-decay data are reduced for $dP_0 = p_{up^0} - p_{down^0}$, $dP_t = p_{up} - p_{down}$ and P_{eq}. A typical set of observations is used for the calculation of uncertainty in the permeability. More details of the analysis and error propagation may be found elsewhere (Kumar et al., 2012). However, the pressure pulse test may show erroneous results if the condition of linear pressure gradient at all times violates (Bourbie and Walls; Hsieh et al., 1981). The aperture of artificial fracture is significantly bigger than the mean free path of the gases used here therefore the possibility of Klinkenberg effect can be eliminated for these experiments. In addition to the permeability data, the evolution of roughness of the fracture surfaces was recovered from micrographs obtained by optical profilometry and reduced using MetroPro. The surface roughness and the indentation into the surface were quantified.

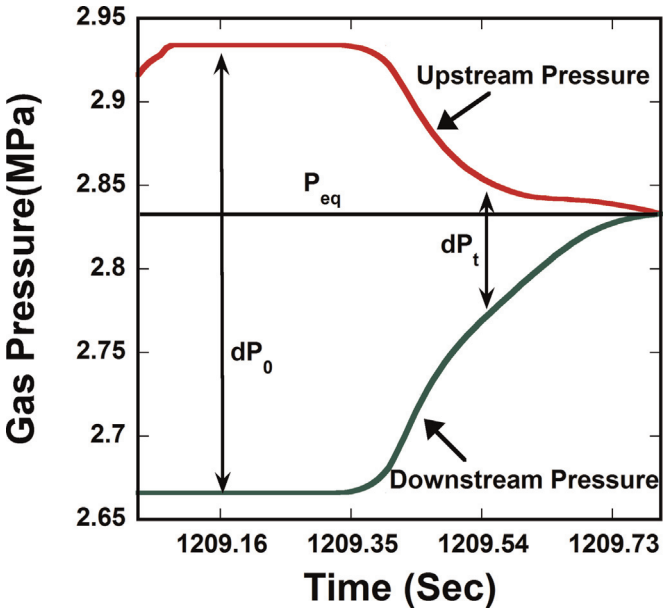

Fig. 3. A typical transient pulse test response for a proppant filled fracture with helium gas.

3. Results and discussion

The permeability experiments for He and CO_2 were conducted at constant total stress of 10 MPa while gas pressures were varied within the range given in Table 1. The permeability of the artificial fracture in coal is modulated by the combined effects of effective stress and swelling/softening. This enables the evolution of permeability to be determined in coal as a function of both gas pressure (swelling/softening) and effective stress.

Smooth artificial fracture surfaces were prepared in split-core-plugs of bituminous and anthracite coals. The permeability evolution was followed for both non-propped and propped fractures with varying gas pressures as a proxy for changing effective stresses and with two gases He and CO_2 as shown in Fig. 4a and 4b. The He permeability of the propped fracture is $\sim$10-fold that of the non-propped fracture in both bituminous and anthracite coal (Fig. 4a and 4b). The permeability of the artificial fracture increases exponentially with decreasing effective stress in non-propped and propped conditions. In the non-propped fracture, the permeability increases three-fold while it increases only two fold in propped fracture when the gas pressure is increased from 2 MPa to 4 MPa indicating that the rate of increase in the permeability being faster

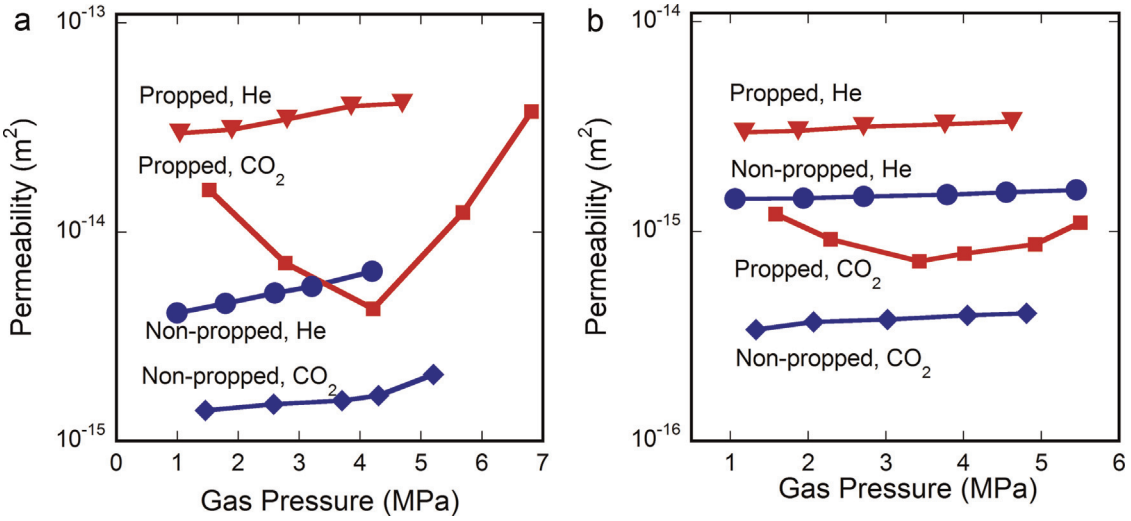

Fig. 4. The permeability evolution of non-propped and propped fracture on injection of He and CO_2 (a) bituminous coal and (b) anthracite coal. The observations are reported at 10 MPa of constant confining stress. The plots are drawn on log–normal axes.

in non-propped fracture relative to that in propped fracture (Fig. 4a) in bituminous coal. This observation in bituminous coal may be attributed to its lower stiffness, which causes surface-deformation possibly by proppant embedment. Notably, coal swelling is not likely to cause on He injection. Therefore, surface deformation due to change in effective stress may play a major role in modulating the permeability on injection of He in coal. The change in permeability on injection of He in anthracite coal under non-propped and propped condition is similar i.e. the permeability increases two fold if the gas pressure is increased from 1 MPa to 5 MPa. This observation in anthracite coal indicates that the proppant embedment does not occur due to its higher stiffness unlike in the case of bituminous coal. These experiments were performed at constant confining stress of 10 MPa (Table 1). We eliminate the possibility of proppant crushing under these conditions given the relative strengths of sand and coal.

The CO_2 permeability evolutions in non-propped and propped artificial fractures for bituminous and anthracite coal are shown also in Fig. 4a and 4b respectively. The CO_2 permeability of non-propped fracture increases with gas pressure in both bituminous and anthracite coal however the CO_2 permeability of intact coals first decreases and then increases exhibiting a "U-shape" pattern with increasing gas pressure (Fig. 4). The increase in gas pressure of sorptive gas under constant confining stress in *intact coal* induces swelling resulting in permeability decrease. But, at a gas pressure greater than the saturation pressure, the decrease in permeability halts and the permeability starts increasing due to the effect of diminishing effective stresses (Kumar et al., 2012). However, non-propped fractures do not demonstrate this behavior (Wang et al., 2011) instead they follow the trend in oversaturated region as observed by Kumar et al. (2012). Our observations are consistent with previous results on fractured coal on injection of CO_2 at constant confining stress (Wang et al., 2011) (Fig. 4). Presumably, the absence of rock bridges (Izadi et al., 2011) in the smooth artificial fracture allows the effect of diminishing effective stress taking over the effect of swelling immediately which results in permeability increase with gas pressure at constant confining stress. The CO_2 permeability of propped fracture in bituminous coal is as high as 10–100 fold and in anthracite coal it is ~10 fold that of the non-propped fractures in the respective coals depending upon the conditions. Interestingly, the permeability evolution in propped fractures exhibit behavior similar to the intact coal. The increase in gas pressure decreases the permeability which halts at certain threshold pressure referred to as saturation pressure and then increases at a pressure greater than the saturation pressure in both bituminous and anthracite coal. The permeability evolution curve with gas pressure shows a point of inflection in both bituminous and anthracite coal (Fig. 4). The magnitude of change in permeability for the propped fracture was higher than that for the non-propped fracture. Intuitively, these observations may be explained by either swelling of the coal or by proppant embedding in the increasingly softer coal due to the presence of sorbing gas (Kumar et al., 2012), or a combination of the two phenomena. It is important to note that these experiments are extreme case of fracture embedment as only monolayer of proppant was sandwiched in the fracture. The effect on permeability due to proppant embedment may be significantly small in larger aperture fractures as multiple proppant layers are expected. The multilayer of proppant would register the permeability equivalent to a sand-bed until the fracture is near closing.

The permeability evolution in non-propped and propped fracture in anthracite coal was found similar to the bituminous coal however the magnitude of change is anthracite coal is smaller in all the cases discussed above. This occurs as the physical properties e.g. coal hardness, initial permeability, pore structure, sorptive capacity/strain etc. of anthracite coal are significantly different than bituminous coal. The quantification of surface indentation in CO_2 injection experiments is explored in later sections of the paper.

4. Analysis

In the following section, a mechanistic model was developed which includes important processes occurring in propped artificial fracture during CO_2 injection. Further, the experimental observations of permeability evolution are utilized to constrain the model. The quantification of the proppant indentation was quantified using an optical profilometer.

4.1. Mechanistic model

A mechanistic model for permeability evolution was developed based on observations in an artificial fracture under non-propped and propped condition in stress-constrained coal. The permeability of an artificial fracture under non-propped and propped condition has been assumed much higher than the coal matrix. In the proposed model, proppant grains are assumed to be acting as

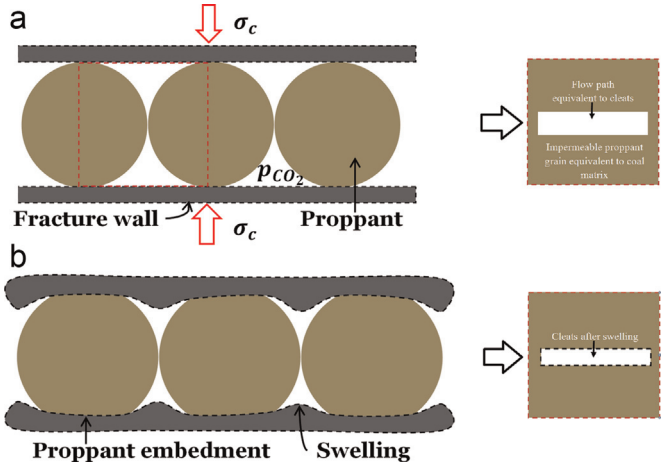

Fig. 5. The sorption induced swelling and normal stress driven embedment is shown. A single unit is shown in red dashed lines (a) before the application of normal stress and sorptive gas pressure and (b) after proppant embedment and swelling. (For interpretation of the references to color in this figure legend, the reader is referred to the web version of this article.)

rock-bridges embedded into the coal matrix. The permeability evolution of the 'matrix embedded rock-bridge' system (Fig. 5a) depends on the processes namely sorption/desorption resulting in swelling/shrinkage of matrix and the change in effective stress leading to proppant embedment/proppant retreat (Fig. 5b). These processes directly modulate the cleat permeability by changing the cleat aperture (Izadi et al., 2011; Tao et al., 2012).

An idealized fracture consisting of two parallel surfaces isolated with sandwiched proppant grains (Fig. 5a) has been assumed for the development of permeability model. The void volume available for flow (CO_2) changes with overburden stress and swelling in turn affecting the permeability. Note that the Fig. 5 is an exaggerated schematic of a proppant filled artificial fracture. A monolayer of proppant is sandwiched in the fracture is shown. The proppant grain might embed into the fracture wall as the normal stress increases or the coal softens on exposure to sorptive gas (e.g. CO_2). Further, CO_2 may swell the coal leading to blocking of flow pathways for the fluid.

The mechanistic model developed here assumes that the permeability modulates as a function of proppant embedment and sorption induced swelling (Kumar et al., 2015). The mathematical formulation is presented below.

The embedded radius of a hard sphere (proppant) pressed against a flat surface (coal fracture surface) can be represented (Bower et al., 1993; Jamari and Schipper, 2005; Mesarovic and Fleck, 2000) (Fig. 6),

$$r_1 = R\sqrt{\frac{\sigma'}{\pi c}} \tag{3}$$

Here r_1 is the radius of the portion (circular) embedded into the surface, R is the radius of proppant grain, σ' is the effective stress and c is the cohesive strength of coal.

The embedded height (h_1) of sandwiched proppant grain,

$$h_1 = R\left(1 - \sqrt{1 - \frac{\sigma'}{\pi c}}\right) \tag{4}$$

The total volume V_1 of proppant grain embedded into the two fracture surfaces can be calculated as

$$V_1 = 2\frac{1}{3}\pi h_1^2(3R - h_1) \tag{5}$$

Consider a cubical unit of coal of side $2R$ containing a proppant grain as shown in Fig. 5 with red dashed lines. The volumetric strain developed in this unit due to sorption-induced swelling may be written as

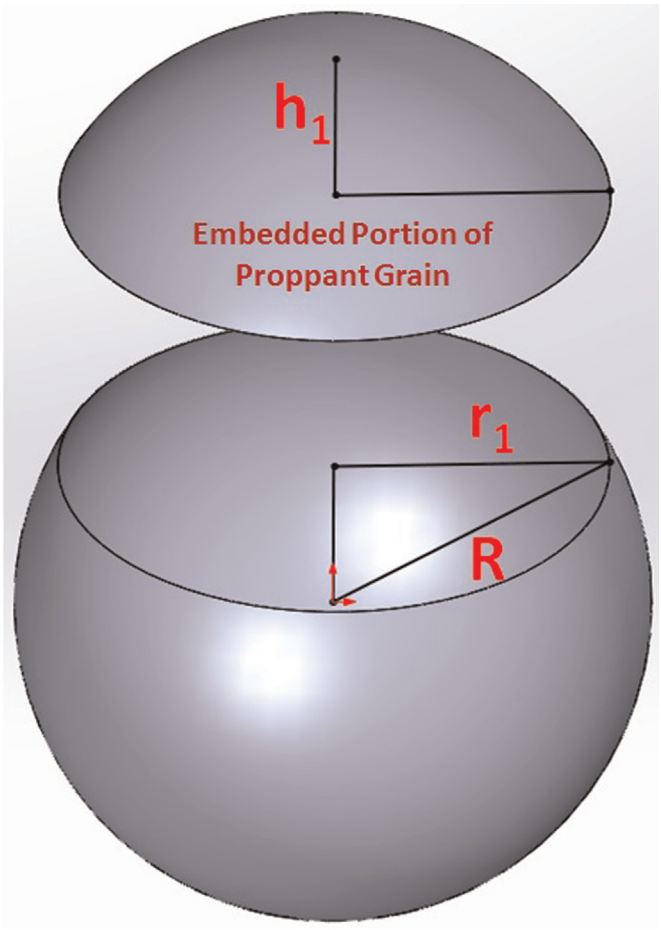

Fig. 6. Three dimensional cartoon (highly exaggerated) of a proppant grain particle. The top portion shows the embedded part.

$$\Delta V = \alpha\varepsilon_L\left(\frac{P}{P + P_L}\right)(2R)^3 \tag{6}$$

Here ΔV is the volumetric strain developed through swelling, α is a arbitrary shape factor, P is the gas pressure of gas and P_L is the Langmuir pressure. The arbitrary shape factor is an index to measure the local volume of coal affected by sorptive gas injection (Liu et al., 2011).

If h_2 is the resultant new embedded height due to stress and swelling then the change in embedded volume can be represented as

$$2\frac{1}{3}\pi h_2^2(3R - h_2) = V_1 + \Delta V \tag{7}$$

$$2\frac{1}{3}\pi h_2^2(3R - h_2) = 2\frac{1}{3}\pi h_1^2(3R - h_1) + \alpha\varepsilon_L\left(\frac{P}{P + P_L}\right)(2R)^3 \tag{8}$$

The new embedded height h_2 can be calculated from Eq. (8). The Eq. (8) is a non-linear equation therefore Microsoft Excel® solver is used to find the solution for h_2 for each value of gas pressure. The effective aperture of fracture b at any point during varying gas pressure at constant confined stress can be written as

$$b = 2R - h_2 = b_0 - \Delta b \tag{9}$$

Here b_0 is the initial fracture aperture.

The change in aperture of the fracture Δb driven by these processes may be represented as

$$\Delta b = -\Delta h_2 \tag{10}$$

For the cases where bulk in situ permeability k_0 is known at fracture aperture b_0 then the permeability evolution with change in aperture can be evaluated (Liu et al., 1997). This allows the evolution of fracture permeability to be followed for an arbitrary evolution of fracture aperture (Elsworth and Goodman, 1986; Piggott and Elsworth, 1993). It has been assumed that flow occurs in fractures only. The permeability of fracture k is modulated based upon its initial permeability k_0 as follows:

$$\frac{k}{k_0} = \left(1 + \frac{\Delta b}{b_0}\right)^3 \tag{11}$$

The formulation allows the evolution of normalized permeability to be represented with change in fracture aperture. The arbitrary shape factor (α) and cohesive strength (c) of coal are evaluated from the best fit as indexed by the coefficient of correlation (R^2). Here it is important to note that the change in aperture of the propped fracture Δb would govern the permeability evolution presented in Fig. 4. Notably, the mechanistic model developed here predicts the permeability evolution only in the case where monolayer proppant is sandwiched in the fracture. We have not evaluated this model for field case hydraulic fracture stimulation.

4.2. Parameter optimization

The mechanistic model developed (Eq. (11)) has been used to describe the permeability evolution in propped fracture in coals on injection of CO_2. The model predicts the permeability with change in combined response to normal stress and sorptive gas pressure in the fractured core. The permeability evolution may be approximated by an arbitrary shape factor and cohesive strength of coal. The numerical values of Langmuir strain and Langmuir pressure are obtained from the literature for bituminous and anthracite coal (Kumar et al., 2012; Robertson, 2005; Wang et al., 2011). Here Langmuir strain is defined as the maximum swelling induced strain in coal due to gas pressure. The value of Langmuir strain and Langmuir pressure are 10% and 0.4 MPa for bituminous coal and 1% and 0.4 MPa for anthracite coal (Kumar et al., 2012). The initial permeability (k_0) and fracture aperture (b_0) have been chosen at first point of observation in permeability experiments in each coal. Therefore, the values of k_0 are different for the bituminous and anthracite coal.

Table 2
The values of fitting parameters used in permeability evolution model in Fig. 7.

Coal type	α	c (MPa)
Bituminous	1.25	4
Anthracite	0.43	5

MATLAB® curve fit toolbox was used to optimize the values of the parameters α and c. This function utilizes the lsqcurvefit algorithm to find the best possible set of values under prescribed constraints (MATLAB Curvefit Toolbox, 2009). The fitting parameters α and c have been obtained for each coal core. The model has been validated for each coal with experimental permeability evolution data in Fig. 7.

The bituminous coal sample has a larger shape factor than the Anthracite coal attributable to its inherent swelling ability on CO_2 exposure (Kumar et al., 2012; Wang et al., 2011). Commonly, the bituminous coal also has more open porosity relative to anthracite (Rogers, 1994) due to which injection gas can travel faster in bituminous coal matrix accessing more pores and inducing higher swelling strain resulting in higher shape factor. Often, the anthracite coal shows higher uniaxial compressive strength (UCS) than that of bituminous coal (Rogers, 1994). Therefore, the anthracite coal was expected to exhibit higher cohesive strength as indicated in Table 2. The values predicted from curve fitting lie within the range of values reported elsewhere (Martin and Maybee, 2000). Unfortunately, no direct comparison of cohesive strength values can be made due to the absence of published data for cohesive strength of these coals under the experimental conditions used in this work.

The permeability of propped fracture reduces as the gas pressure of the sorbing gas augments in steps at constant confining stress. The reduction in permeability is caused by the coal swelling and/or proppant embedment that reduce the pathways in the propped fracture. As the peak swelling strain is approached, the reduction in permeability halts and permeability increases with gas pressure (Fig. 7) making a “U-shape”. The “U-shape” was observed in both bituminous and anthracite coal at different gas pressure corresponding to maximum swelling strain. The maximum swelling strain in bituminous coal is an order of magnitude higher than that of anthracite coal leading to larger permeability reduction bituminous coal. The maximum reduction in permeability is 27% and 6% for bituminous and anthracite coal respectively. The distinct difference in permeability-reduction is

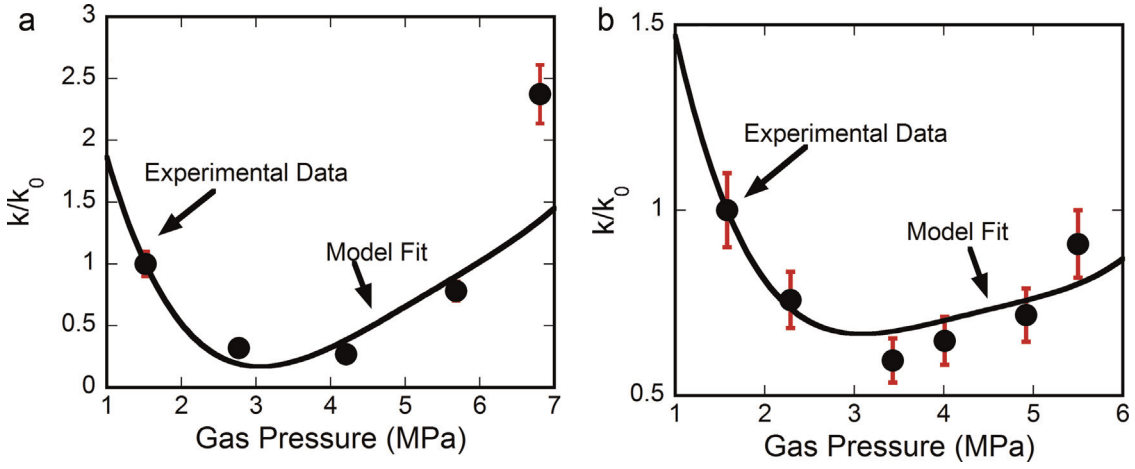

Fig. 7. The evolution of permeability in propped fracture on injection of CO_2. The model fit is shown with black solid line (a) bituminous coal and (b) anthracite coal. The uncertainty in permeability measurement is show by error bar ($\pm$ 10%) at each observation.

attributable to swelling which occurs due to CO_2 uptake capacity and swelling induced strain. The reduction in permeability halts when infiltrating gas pressure becomes approximately equal to the pressure at which maximum adsorption strain occurs. If the gas pressure is further increased then the fracture dilates leading to permeability increase (Fig. 7).

This mechanistic model represents the modulation of propped fracture permeability where swelling and effective stress plays a major role. The excellent fit of the model to the permeability evolution observations in various ranks coal shows the model consistency and plausibility. To the best of our knowledge, no current model presents the mechanistic explanation to the permeability evolution in propped fracture on injection of sorbing gas.

4.3. Quantification of surface indentation

White light optical profilometry was utilized to quantify and characterize the surface of the polished coal. High magnification three-dimensional surface micrographs were obtained and stitched together to obtain a 7 mm × 4.5 mm area. The surface characteristics are compared using micrographs before and after the experimental suite. Same core was used for propped and non-propped experiments.

The coal surface is relatively smooth from the polishing process but with the surface being slightly elevated at places (Fig. 8). The coal consists of microlithotypes varying in their microhardness (Bratek et al., 2002; Das, 1972; Hower et al., 2008; Loustalet et al., 1994; Mukherjee et al., 1989; Nandi et al., 1977), sorption capacity (Laxminarayana and Crosdale, 2002; Richard, 2012; Weniger et al., 2012) and swelling strain (Kiyama et al., 2011; Yang and Zoback, 2011). The hard lithotypes (vitrain) remains elevated on the coal surface compared to the softer lithotypes (clarain) after polishing of the surface. This occurs due to differences in micro-hardness of different lithoptypes. The height differences are visually enhanced using false coloring where elevated features are shown by bright colors and other features are accordingly color coded. The topology changes are evident in the surface before and after the experimental suite (Fig. 8). The surface roughness of polished fractures were 1.09 μm and 0.90 μm for bituminous and anthracite coal respectively. The smooth surface of the fracture was slightly rougher after exposure to 1.24 μm and 1.43 μm respectively probably due to a slight irreversible structural rearrangement within the coal with CO_2 uptake and loss. The infrequent depressed features are pits caused by proppant indentation most likely caused by a non-monolayer distribution of the sand. Coal softening would be expected to produce multiple evenly spaced pits. Thus, for the bituminous coal at these conditions no evidence of coal softening was observed. Thus, coal swelling and the management of the injection system should remain the research focus. Although, the fracture roughness may affect the swelling and embedment but this research work does not investigate these effects. This can be addressed by future research work.

Pre-existing pitting is likely due to mineral grain removal during polishing. The histogram plots of feature height before and after the experimental suite are shown in Fig. 9. The distribution of feature height is wider and smoother (Fig. 9) for the fracture surface before the experimental suite indicating smooth surface prior to the experiments.

A suitable location was been chosen to quantify the surface indentation on the coal surface in anthracite coal. A single pit on fracture surface was analyzed using a 50 × objective lens in optical profilometer. An area of 1.18 mm × 0.67 mm was captured at high magnification with dual light level in auto focus mode. Twenty small micrographs are attached to quantify the surface indentation by proppant grain. The micrographs show a deep pit surrounded by relatively elevated regions (Fig. 10). The region colored in black indicates a deep and/or non-reflective surface, which was beyond the measurement capability of profilometer. The depth of the pit is 60 μm from the surface of the coal which is ~(1/3)rd of the mean particle size of the proppant. Had coal softening occurred, it would have reduced the coal stiffness more uniformly, which would increase the areal density of pits on the fracture surface. On the contrary, the pits observed are infrequent and isolated, indicating insignificant contribution of coal softening under these conditions towards reduction in permeability. However, the uniformly distributed elevated features present on the fracture surface post the experiments (Fig. 8) indicate coal swelling to be the likely contributor to the permeability reduction. The future work in this area may investigate the effect of fracture roughness on swelling and embedment.

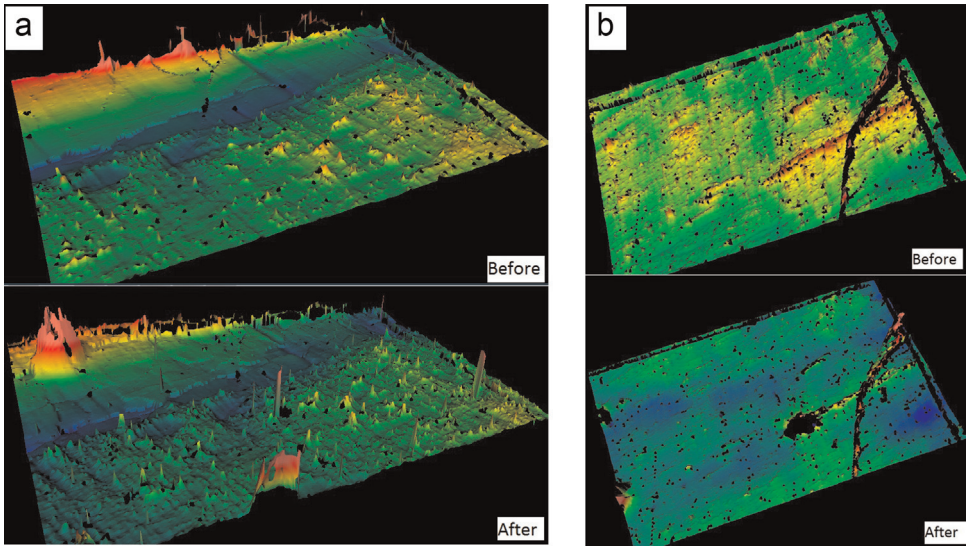

Fig. 8. The aerial view of coal surface before (top) and after (bottom) the experiment (a) bituminous and (b) anthracite. The vertical features are highly exaggerated (on the order of several microns) and are falsely colored. The red color represents highest elevated part while blue shows the depressed features on coal surface. The black regions indicate poorly reflecting deep pits which receives/sends poor signals during profilometer scanning. The region of interest shown is 7 mm × 5 mm (i.e. the vertical and horizontal scales differ by several orders of magnitude). (For interpretation of the references to color in this figure legend, the reader is referred to the web version of this article.)

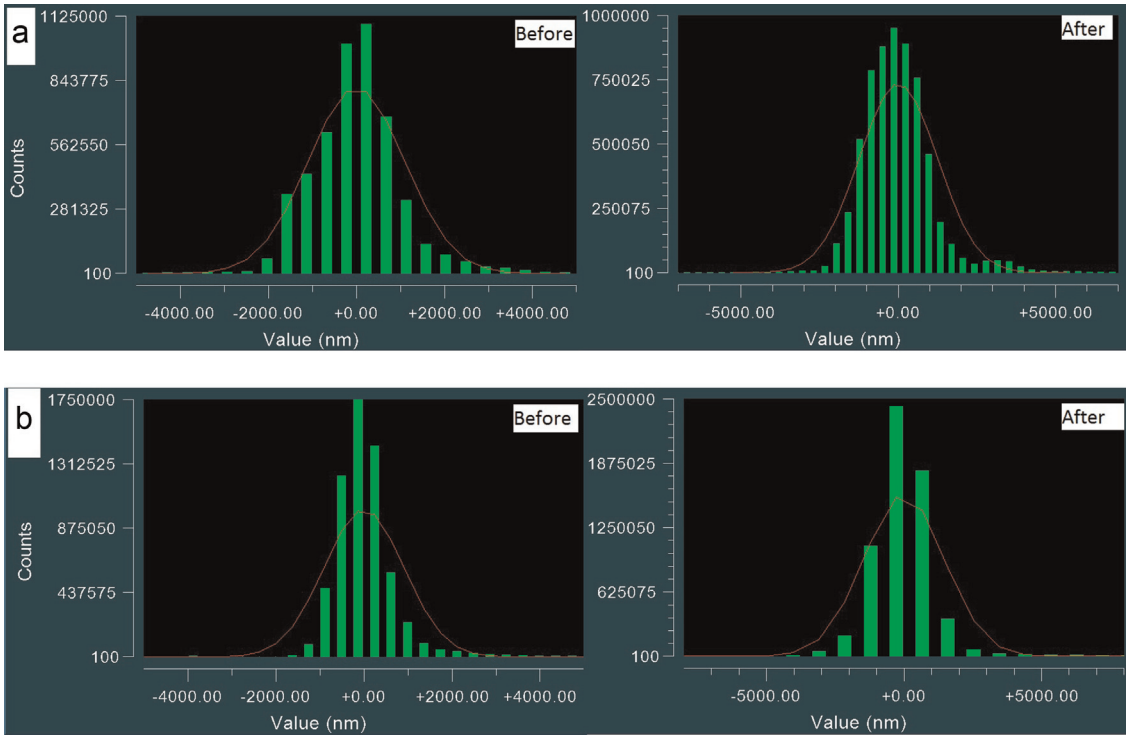

Fig. 9. The surface histograms before and after the experimental suite for (a) bituminous and (b) anthracite coal. The histograms represent the number of features of same height on the *y*-axis with their characteristics height from the mean on the *x*-axis. The negative height represents the depressed regions from mean surface height.

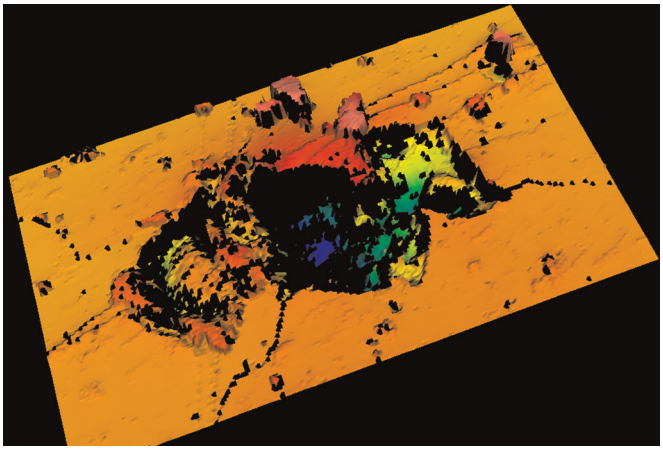

Fig. 10. A false colored high resolution micrograph capturing an area of 1.18 mm × 0.67 mm on the fracture surface after the experimental suite. The region in black color is an example of surface indentation by proppant. (For interpretation of the references to color in this figure legend, the reader is referred to the web version of this article.)

5. Conclusions

The permeability evolution was investigated for saw cut idealized fracture in bituminous and anthracite coal with injection of both non-sorptive (He) and sorptive gases under mechanically constrained condition. The permeability evolution for the same fracture was explored under propped conditions. We consider an extreme case of proppant placement in fracture i.e. a uniform monolayer. The following observations and conclusions are proposed.

1. The permeability of non-propped and propped artificial fracture increases on injection of He at constant confining stress of 10 MPa in both bituminous and anthracite coal. This increase may be 2–3 times if the gas pressure is increased from 1 MPa to 5 MPa. Notably, the bituminous coal shows higher change in permeability with effective stress due to its lower stiffness.
2. The increase in He permeability may be as high as ~10 fold in bituminous and ~5 fold in anthracite if monolayer proppant is sandwiched in the coal fracture. Similar increase is observed in the case of sorptive gas (CO_2) permeability.
3. The CO_2 permeability of non-propped artificial coal fracture increases with gas pressure in both coals. However, the permeability evolution with CO_2 exposure exhibits a "U-shape" pattern with gas pressure at constant confining stress in the propped fracture. The permeability decreases (likely due to coal swelling) and then increases (likely due to diminishing effective stresses) with effective stress. The permeability reduction with gas pressure is caused by coal swelling and coal softening was eliminated as a possible mechanism of permeability reduction. The permeability evolution in propped artificial fracture on injection of CO_2 exhibits a deeper "U-shape" in bituminous coal which may be attributed to its higher swelling strain and stiffness in comparison to anthracite coal.
4. A mechanistic model was developed for permeability evolution in propped fracture under CO_2 injection. Primarily, the permeability modulates as the swelling and effective stress varies with gas pressure. The model yields acceptable match with the experimental observations.
5. The roughness of fracture surface increases due to surface indentation and coal swelling. The pits created on fracture surface are significant ~(1/3)rd compared to proppant size.

Acknowledgments

This work is as a result of partial support from ConocoPhillips. This support is gratefully acknowledged. The authors acknowledge

the contribution of Josh Stapleton at Material Research Institute at Penn State University for optical profilometer analysis.

References

ASTM International D388, 2005. Standard Classification of Coals by Rank. IHS, Pennsylvania, United States.

ASTM International D3302/D3302M-10, 2010. Standard Test Method for Total Moisture in Coal. IHS, Pennsylvania, USA, D3302/D3302M -10.

ASTM International D5671, 2011. Standard Practice for Polishing and Etching Coal Samples for Microscopical Analysis by Reflected Light. IHS.

ASTM International D7582, 2010. Standard Test Methods For Proximate Analysis of Coal and Coke by Macro Thermogravimetric Analysis. IHS, Pennsylvania.

Bai, M., Elsworth, D., 1994. Modeling of subsidence and stress-dependent hydraulic conductivity for intact and fractured porous media. Rock Mech. Rock Eng. 27 (4), 209–234.

Bourbie, T., Walls, J., Pulse Decay Permeability: Analytical Solution and Experimental Test.

Bower, A.F., Fleck, N.A., Needleman, A., Ogbonna, N., 1993. Indentation of a Power Law Creeping Solid. Proc. R. Soc. Lond. A 441 (1911), 97–124.

Brace, W.F., Walsh, J.B., Frangos, W.T., 1968. Permeability of granite under high pressure. J. Geophys. Res. 73 (6), 2225–2236.

Bratek, K., Bratek, W., Gerus-Piasecka, I., Jasienko, S., Wilk, P., 2002. Properties and structure of different rank anthracites. Fuel 81 (1), 97–108.

Brenner, D., 1984. Microscopic in-situ studies of the solvent-induced swelling of thin sections of coal. Fuel 63, 1324–1328.

Brenner, D., 1985. The macromolecular nature of bituminous coal. Fuel 64 (2), 167–173.

Das, B., 1972. Microhardness of abnormally metamorphosed coal. Fuel 51 (1), 52–53.

Davidson, R.M., Sloss, L.L., Clarke, L.B., 1995. Coalbed Methane Extraction. IEA Coal Research, London.

Elsworth, D., Goodman, R.E., 1986. Characterization of rock fissure hydraulic conductivity using idealized wall roughness profiles. Int. J. Rock Mech. Min. Sci. 23 (3), 233–244.

Elsworth, D., Yasuhara, H., 2010. Mechanical and transport constitutive models for fractures subject to dissolution and precipitation. Int. J. Numer. Anal. Methods Geomech. 34 (5), 533–549.

Freeman, E.R., Anschutz, D.A., Rickards, A.R., Callanan, M.J., 2009. Modified API/ISO crush tests with a liquid-saturated proppant under pressure incorporating temperature, time, and cyclic loading: what does it tell us? SPE Hydraulic Fracturing Technology Conference. Society of Petroleum Engineers, The Woodlands, Texas.

Holditch, S.A., Ely, J.W., Semmelbeck, M.E., Carter, R.H., 1988. Enhanced Recovery of Coalbed Methane Through Hydraulic Fracturing. SPE Annual Technical Conference and Exhibition. SPE, Houstan, Texas, pp. 43.

Hower, J.C., Trinkle, E.J., Raione, R.P., 2008. Vickers microhardness of telovitrinite and pseudovitrinite from high volatile bituminous Kentucky coals. Int. J. Coal Geol. 75 (2), 76–80.

Hsieh, P.A., Tracy, J.V., Neuzil, C.E., Bredehoeft, J.D., Silliman, S.E., 1981. A transient laboratory method for determining the hydraulic properties of 'tight' rocks–I. Theory. Int. J. Rock Mech. Min. Sci. Geomech. Abstr. 18 (3), 245–252.

Izadi, G., et al., 2011. Permeability evolution of fluid-infiltrated coal containing discrete fractures. Int. J. Coal Geol. 85 (2), 202–211.

Jamari, J., Schipper, D.J., 2005. Experimental investigation of fully plastic contact of a sphere against a hard flat. J. Tribol. 128 (2), 230–235.

Karacan, C.Ö., 2003. Heterogeneous sorption and swelling in a confined and stressed coal during CO_2 injection. Energy Fuels 17 (6), 1595–1608.

Karacan, C.Ö., 2007. Swelling-induced volumetric strains internal to a stressed coal associated with CO_2 sorption. Int. J. Coal Geol. 72 (3–4), 209–220.

Kiyama, T., et al., 2011. Coal swelling strain and permeability change with injecting liquid/supercritical CO_2 and N_2 at stress-constrained conditions. Int. J. Coal Geol. 85 (1), 56–64.

Kumar, H., Elsworth, D., Liu, J., Pone, D., Mathews, J.P., 2011. Optimization of CO_2-enhanced coalbed methane recovery accommodating swelling-induced permeability evolution. American Geophysical Union, Fall Meeting 2011.

Kumar, H., Elsworth, D., Liu, J., Pone, D., Mathews, J.P., 2012. Optimizing enhanced coalbed methane recovery for unhindered production and CO_2 injectivity. Int. J. Greenh. Gas Control 11 (0), 86–97.

Kumar, H., Elsworth, D., Mathews, J.P., Liu, J., Pone, D., 2014. Effect of CO_2 injection on heterogeneously permeable coalbed reservoirs. Fuel 135 (0), 509–521.

Kumar, H., Elsworth, D., Mathews, J.P., Marone, C., 2015. Permeability evolution in sorbing media: analogies between organic-rich shale and coal. Geofluids.

Kumar, H., Pone, J.D.N., Mitchell, G.D., Halleck, P.M., Mathews, J.P., 2009. Lithotype influences on (an idealized) coal cleat surface deformation by carbon dioxide induced coal swelling. International Coalbed Methane and Oil Shale Symposium. Tuscaloosa, Alabama.

Lacy, L.L., Rickards, A.R., Ali, S.A., 1997. Embedment and fracture conductivity in soft formations associated with HEC, borate and water-based fracture designs. SPE Annual Technical Conference and Exhibition. San Antonio, Texas, pp. 255–268.

LaFollette, R.F., Carman, P.S., 2010. Proppant diagenesis: results so far. SPE Unconventional Gas Conference. Society of Petroleum Engineers, Pittsburgh, Pennsylvania, USA.

Laxminarayana, C., Crosdale, P.J., 2002. Controls on methane sorption capacity of Indian coals. AAPG Bull. 86 (2), 201–212.

Lee, D.S., Elsworth, D., Yasuhara, H., Weaver, J.D., Rickman, R., 2010. Experiment and modeling to evaluate the effects of proppant-pack diagenesis on fracture treatments. J. Pet. Sci. Eng. 74 (1–2), 67–76.

Liu, J., Elsworth, D., Brady, B.H., 1997. Analytical evaluation of post-excavation hydraulic conductivity field around a tunnel. Int. J. Rock Mech. Min. Sci. 34 (3–4), 181.e1–181.e7.

Liu, J., et al., 2011. Impact of transition from local swelling to macro swelling on the evolution of coal permeability. Int. J. Coal Geol. 88 (1), 31–40.

Loustalet, D., Oberlin, A., Moreau, M., 1994. Peculiar process of coal–tar pitch. Carbonization (textural and physicochemical characterization). Carbon 32 (7), 1267–1275.

Martin, C.D., Maybee, W.G., 2000. The strength of hard-rock pillars. Int. J. Rock Mech. Min. Sci. 37 (8), 1239–1246.

Mesarovic, S.D., Fleck, N.A., 2000. Frictionless indentation of dissimilar elastic–plastic spheres. Int. J. Solids Struct. 37 (46–47), 7071–7091.

Mukherjee, A.K., Alam, M.M., Ghose, S., 1989. Microhardness characteristics of Indian coal and lignite. Fuel 68 (5), 670–673.

Nandi, B.N., Ciavaglia, L.A., Montgomery, D.S., 1977. The variation of the microhardness and reflectance of coal under conditions of oxidation simulating weathering. J. Microsc. 109 (1), 93–103.

Perera, M.S.A., Ranjith, P.G., 2012. Carbon dioxide sequestration effects on coal's hydro-mechanical properties: a review. Int. J. Energy Res. 36 (10), 1015–1031.

Piggott, A.R., Elsworth, D., 1993. Laboratory assessment of the equivalent apertures of a rock fracture. Geophys. Res. Lett. 20 (13), 1387–1390.

Pope, C., Peters, B., Benton, T., Palisch, T., 2009. Haynesville shale – one operators approach to well completions in this evolving play. SPE Annual Technical Conference and Exhibition. Society of Petroleum Engineers, New Orleans, Louisiana.

Richard, S., 2012. Relationships between CO_2 sorption capacity by coals as measured at low and high pressure and their swelling. Int. J. Coal Geol. 90–91 (0), 156–161.

Robertson, E.P., 2005. Measurement and Modeling of Sorption-induced Strain and Permeability Changes in Coal. Idaho National Laboratory, Idaho, INL/EXT-06-11832.

Rogers, R.E., 1994. Coalbed Methane: Principles and Practice. PTR Prentice Hall, Englewood Cliffs, N.J.

Rousseau, D., Sonwai, S., Khan, R., 2010. Microscale surface roughening of chocolate viewed with optical profilometry. J. Am. Oil Chem. Soc. 87 (10), 1127–1136.

Stoddard, T., McLennan, J., Moore, J., 2011. Fracture conductivity of a bauxite-propped geothermal system at in-situ conditions. In: Proceedings of the Thirty-sixth Workshop on Geothermal Reservoir. Engineering Stanford University, Stanford, California.

Tao, S., et al., 2012. Dynamic variation effects of coal permeability during the coalbed methane development process in the Qinshui Basin, China. Int. J. Coal Geol. 93 (0), 16–22.

Terracina, J.M., Turner, J.M., Collins, D.H., Spillars, S., 2010. Proppant selection and its effect on the results of fracturing treatments performed in shale formations. SPE Annual Technical Conference and Exhibition. Society of Petroleum Engineers, Florence, Italy.

Viete, D.R., Ranjith, P.G., 2006. The effect of CO_2 on the geomechanical and permeability behaviour of brown coal: implications for coal seam CO_2 sequestration. Int. J. Coal Geol. 66 (3), 204–216.

Walsh, J.B., 1981. Effect of pore pressure and confining pressure on fracture permeability. Int. J. Rock Mech. Min. Sci. Geomechan. Abstr. 18 (5), 429–435.

Wang, S., Elsworth, D., Liu, J., 2011. Permeability evolution in fractured coal: the roles of fracture geometry and water content. Int. J. Coal Geol. 87 (1), 13–25.

Weniger, P., Francü, J., Hemza, P., Krooss, B.M., 2012. Investigations on the methane and carbon dioxide sorption capacity of coals from the SW Upper Silesian Coal Basin, Czech Republic. Int. J. Coal Geol. 93 (0), 23–39.

Yang, Y., Zoback, M.D., 2011. The Effects of Gas Adsorption on Swelling, Visco-plastic Creep and Permeability of Sub-bituminous Coal. ARMA, American Rock Mechanics Association, San Francisco.

Yasuhara, H., Elsworth, D., 2008. Compaction of a rock fracture moderated by competing roles of stress corrosion and pressure solution. Pure Appl. Geophys. 165 (7), 1289–1306.

Yasuhara, H., et al., 2006. Evolution of fracture permeability through fluid–rock reaction under hydrothermal conditions. Earth Planet. Sci. Lett. 244 (1–2), 186–200.